THE ASTROPHYSICAL JOURNAL, 337:236–250, 1989 February 1

HOT DUST ON THE OUTSKIRTS OF THE BROAD-LINE REGION IN FAIRALL 9[1]

J. CLAVEL[2] AND W. WAMSTEKER[2]
ESA *IUE* Observatory, Madrid, Spain
AND
I. S. GLASS
South African Astronomical Observatory
Received 1988 February 10; accepted 1988 July 7

ABSTRACT

Since 1978, the Seyfert 1 galaxy F9 has been observed 54 times in the far-ultraviolet and optical (FES) range with the *IUE*, and at 27 different epochs at *J*, *H*, *K*, and *L*. The UV continuum underwent dramatic variations, its intensity decreasing by a factor 33, from a maximum in 1978 to a deep minimum in mid-1984.

The near-IR and optical fluxes changed by a factor of ~ 3 and in the same sense as the ultraviolet. Variations in the optical and *J* band are diluted by starlight but are in phase with those in the UV. This contrasts with the variations at *K* and *L* which are *delayed* by 400 ± 100 days. We interpret the *K* and *L* emission as thermal radiation from dust lying at ~ 1 lt-yr from the UV source. The equilibrium temperature of the grains is 1730 ± 230 K, which implies that they are made of graphite. The mass of hot dust is small and does not contribute significantly to the extinction.

The Lyα λ1216, C IV λ1550, and Mg II λ2800 emission-line intensities also vary in the same sense as the UV continuum but with a lag of 155 ± 45 days. This strongly suggests that the broad-line region (BLR) gas is photoionized and lies at ~ 150 lt-day from the UV source, i.e. inside the dust shell.

Strong correlations exist between the Lyα/C IV and Lyα/Mg II line ratios, on the one hand, and the intensity of the ultraviolet continuum, on the other. This is likely to be due to the factor of ~ 10 increase of the X-ray to UV luminosity ratio which accompanied the 1978–1984 decline of F9. It is probably the strongest evidence to date that the Mg II λ2800 line emissivity depends primarily on the density of soft X-ray photons, as postulated in optically thick photoionization models of the BLR.

Despite large intensity variations, the spectral index of the UV continuum remains constant, $\alpha = -0.46 \pm 0.11$, equivalent to a blackbody temperature $T_{bb} = 26{,}500 \pm 900$ K. The constancy of α or T_{bb} is a new important constraint on models which aim at explaining the origin of the "big blue bump" in AGNs.

Subject headings: galaxies: individual (Fairall 9) — galaxies: Seyfert — infrared: sources — ultraviolet: spectra

I. INTRODUCTION

The origin of the complex shape of the spectral energy distribution (SED) of active galactic nuclei (AGNs) and quasars is still poorly understood.

Typically, non-blazar AGNs display a steep ($\alpha = -1$ to -2, $F_\nu \propto \nu^\alpha$ in units of ergs cm^{-2} s^{-1} Hz^{-1}) infrared power law, with an upturn in the optical and ultraviolet (see Edelson and Malkan 1986, and references therein). The rather flat ($\alpha \sim -0.5$) UV continuum, often referred to as the "big blue bump," must roll over somewhere in the unexplored extreme ultraviolet region so as to connect with the X-ray spectrum which typically lies an order of magnitude below an extrapolation of the ultraviolet on a $\nu - F_\nu$ diagram. A steep soft X-ray excess is detected in several objects (Pravdo and Marshall 1984; Arnaud *et al.* 1985; Singh, Garmire, and Nousek 1985; Elvis, Wilkes, and Tananbaum 1986; Perola *et al.* 1986), possibly including Fairall 9 (Morini *et al.* 1986), which could represent the high-energy tail of this bump. The hard X-ray spectrum is fairly flat ($\alpha \sim -0.7$) and extends to 160 keV and beyond, at least in the few studied cases (Rothschild *et al.* 1983).

[1] Based on *IUE* observations made at the ESA satellite tracking station near Madrid, Spain, and at the NASA Goddard Space Flight Center, Maryland, and on infrared observations made at the South African Astronomical Observatory.

[2] Affiliated with the Astrophysics Division, Space Sciences Department.

Starlight from the host galaxy is an important contributor in the ~ 0.36 to 1–2 μm range in particular in low-luminosity AGNs. In addition, the SED of most Seyfert 2 galaxies and other dusty objects includes a broad hump in the mid- to far-infrared region which has been attributed to warm (~ 60 K) dust emission probably associated with the narrow-line region (Rieke and Lebofsky 1979; Edelson and Malkan 1986). Finally, approximately half of the Seyfert 1 galaxies and QSOs in the sample of Edelson and Malkan (1986) display an additional "3 μm bump," the origin of which is uncertain.

The main purpose of this paper is to present some new results pertinent to the SED of AGNs, and in particular to the origin of the 3 μm bump. More precisely, our observational results show that in at least one object, Fairall 9, the near-IR flux is mostly thermal dust radiation from a compact region just outside the broad-line region (BLR) where the grains are heated to their evaporation temperature, thereby confirming Barvainis's (1987) recent theoretical work. In addition, our data shed light on the temporal behavior and spectral shape of the big blue bump and set constraints on models which aim at explaining its origin. Finally, we obtain a precise determination of the size of the BLR in Fairall 9.

Fairall 9 is a relatively close by ($z = 0.0461$; Weedman 1979) Seyfert 1 galaxy. At the time of its discovery (Fairall 1977), its optical luminosity, $M_v = -24.25$ ($H_0 = 100$ km s^{-1} Mpc^{-1} is used throughout) was typical of QSOs rather than Seyfert 1

TABLE 1

LOG OF *IUE* OBSERVATIONS

Date	JD	SWP#	Texp	LWP/R#	Texp
780618	677	1804,805	120,45	R 1685	45
780628	687	...	...	1744	45
780802	723	2178	45	1954	45
780805	726	2215	120	...	...
790118	891	3936,937	37,25	3511	38
790308	941	4539	45	3959,960	45,25
790323	956	4732	30	...	...
800623	1414	9353,354	35,25	8114	27
800728	1448	9616	25	8382	35
801231*	1605	10941	25	9615	30
810223	1659	13351	135	10000,002	30,90
810330	1694	13616	40	...	...
810602	1757	14157,158	90,60	10761	105
811209	1947	15689	60	...	...
811218	1957	15794,795	45,20	12166,167	40,170
811227	1966	15890	25	12226	40
820222	2022	16410	73	12662	40
820225	2026	16426	40	...	...
820317	2046	16559	60	...	...
820501	2090	...	...	13123	50
820504	2093	16890	90	...	...
820618	2138	17429	70	13514	60
820719	2169	17446	135	13714	105
820730	2180	17521	60	13801	90
820924	2237	18094	40	...	...
821004	2247	18202	40	14334	16
821008	2251	18242	40	...	...
821024	2266	18382	45	...	...
821108	2282	18506	50	14585	50
821225	2329	...	...	14908	70
831009	2618	21260,261	50,115	P 2020,021	50,58
831013	2622	21286,287	120,90	2037,038	120,48
840428	2819	22875	30	...	...
840830	2943	23824	75	4106	60
841017	2991	24193	48	...	...
841021	2995	24254	90	4603	64
841025	2999	24291	120	4639	120
841029	3003	24345	91	...	...
850501	3186	25825	150	5872	208
850725	3272	26479,480	120,110	6491,492	100,80
850928	3327	26774	180	...	...
851101	3370	27007,008	170,83	7022,023	73,69
851227	3426	27399,400	70,163	7396,397	70,40
860412*	3533	28160	70	8017	70
860422	3542	28212,213	50,150	8080,081	50,115
860514	3564	28306,307	60,120	8197	40
860707*	3620	28632,633	120,100	8562	100,60
860811	3654	28891	70	...	...
861025	3729	29528	60	9408	30
861028	3731	29544,545	45,120	9425,426	60,160
861230	3794	29990-992	50,180,55	9823,824	30,60
870124*	3821	30152,160	65,150	10017	60
870508	3924	30933	50,100	10713	30
870616	3963	31175,176		11027	65

NOTES.—First column: date expressed as year, month, day (two digits each) at which the observations started; an asterisk means that they carried over the next day as well. Second column: Julian day:—2,443,000 rounded down to the nearest integer. Third and fifth columns, SWP and LWP (*P*) or LWR (*R*) image sequential number; when more than one spectrum was obtained, only the last three digit(s) of the subsequent image(s) is printed preceded by a comma. Fourth and sixth columns: exposure time in minutes: if several spectra exist, the various exposure times are separated by a comma.

galaxies. After 1978, it entered a long period of decline which ended in 1984 when its ultraviolet flux started to rise again (Wamsteker, Gilmozzi, and Clavel 1985).

II. OBSERVATIONS AND DATA ANALYSIS

All the low-resolution (900 km s^{-1}) large-aperture (10″ × 20″) ultraviolet spectra of Fairall 9 through 1987 July have been retrieved from the *IUE* (Boggess *et al.* 1978) data bank. These amount to a total of 51 epochs of observations with the short-wavelength (SW: 1200–1950 Å) spectrograph and 39 epochs in the long-wavelength (LW: 1900–3200 Å) range. The long-wavelength data were recorded with the LWR camera prior to 1983 October and with the LWP detector afterward. The image sequential numbers are listed in Table 1. Usually, the exposure times were such that the strong Lyα λ1216, C IV λ1550 and Mg II λ2800 emission lines were optimally exposed. For about one-third of the observations, two spectra per wavelength range have been obtained. In such cases, one of these was often intentionally overexposed to bring up the flux level in the much fainter continuum. Unfortunately, in F9, the important C III] 1908 line is redshifted to 1996 Å where the sensitivity of the LW detectors is too low to allow any useful measurement. The majority of the observations were carried out by the authors, but several other *IUE* observers were involved as well. As a result, the observing procedure varied: most of the time the fine error sensor (FES) on board *IUE* was used in its star-tracker mode to center the nucleus of F9 in the spectrograph apertures. On other occasions, offset maneuvering from a nearby star was performed to acquire the target. Both procedures are standard and the choice of one rather than the other had no significant impact on the quality of the UV data. It was possible in the first case to record the FES counts and thus obtain simultaneous measurements of the optical flux of Fairall 9 in a 12″ square aperture. The FES is a reliable photometer whose S-20 photocathode response curve is characterized by a steep onset at ~3600 Å, with a peak at 4600 Å and a smooth quasi-linear decline up to 9000 Å where the zero level is reached again (Holm and Crabb 1979). Its effective wavelength for flat AGN-type energy distribution is ~5200 Å and depends weakly on the relative amount of stellar and nonstellar flux, hence on the intensity. In other words, the optical flux which we measure is mostly that of the continuum near 5200 Å, but includes also a contribution from emission lines, mainly Hβ λ4862. The FES counts were corrected for the 3% per year sensitivity loss which occurred after 1981 (Barrylak, Watasonic, and Imhoff 1985). At each epoch, several FES measurements were usually obtained (one prior to each UV exposure), and only the mean values are listed in Table 2. We have adopted a constant relative error of 6.7% which corresponds to the average of the rms deviations of the individual measurements at each epoch. Systematic errors from epoch to epoch are negligible.

All the ultraviolet data have been processed with the latest version of the *IUE* low-resolution software (Bohlin, Holm, and Lindler 1981). We corrected the LWR spectra for the loss of sensitivity of the LWR detector (Clavel, Gilmozzi, and Prieto 1988). The amount of degradation of the SWP and LWP cameras was deemed too small to be worth compensating for (Sonneborn and Garhart 1987; Bohlin and Grillmair 1988).

The continuum intensity at 1338 and 1826 Å, $F(1338)$ and $F(1826)$ (unless otherwise stated, all wavelengths are expressed in the rest frame of Fairall 9), are listed in Table 2. $F(1338)$ and $F(1826)$ represent the mean (and error on the mean) flux over the 1328–1348 Å and 1810–1840 Å spectral interval, respectively. When more than one spectrum is available, the results have been averaged, and the error was taken to be the mean error or the rms of the individual measurements, whichever is the largest. Our continuum measurements could be affected by weak C II λ1335 and Si II $\lambda\lambda$1808, 1817 emission, although none of these lines are detected in Fairall 9. No other suitable continuum "windows" could be found, owing in particular to the many blended Fe II lines longward of ~2000 Å (Netzer and Wills 1983).

The intensities of the three strongest UV lines, Lyα 1216, C IV λ1550, and Mg II λ2800, Å are given in Table 2. They are measured in a purely impersonal way by summing up all the flux above the continuum in the 1176–1279 Å, 1495–1600 Å, and 2703–2895 intervals, respectively. For Lyα λ1216 and C IV λ1550, the underlying continuum was obtained by linear interpolation between $F(1338)$ and $F(1826)$. In the case of Mg II λ2800, a local continuum was used, whose intensity was chosen to be the mean value of the flux measured in the 2663–2682 Å and 2897–2916 Å intervals. When more than one spectrum is available, the results have been averaged. A 10% relative error was assumed for all three line intensities, corresponding roughly to the rms deviations of individual measurements. As usual, the main source of error comes from the uncertainty in the true location of the continuum. However, being a systematic error, it does not affect our results which are based mainly on relative line intensity variations. Unavoidably, the Lyα λ1216 intensity contains a small contribution from the much weaker N V λ1240 line, whereas some contamination of Mg II λ2800 by Fe II multiplets is also to be expected. An "S" in Table 2 means that the line was saturated.

The infrared *JHKL* data were obtained at the SAAO. The observing procedure, as well as most of the data has been reported elsewhere (Glass 1986). In Table 3, we only list those fluxes not published previously.

Figures 1*a*–1*d* show the light curves of the continuum at 1338 Å, $F(1338)$, in the FES optical band, F(FES), at 2.1 μm, $F(K)$, and of the Lyα λ1216 emission line.

III. RESULTS

a) The Optical-Ultraviolet Continuum

As can be judged from Figure 1, the amplitude of the variations are the largest in the ultraviolet continuum. Hereafter, amplitudes will be quantified with the parameter $f = F_{max}/F_{min}$, i.e. the ratio of the maximum to the minimum value recorded. In the case of the UV continuum, F_{min} was taken to be the average of the three lowest values of $F(1338)$, which allows us to reduce the error on f. With this definition, we obtain $f = 33 \pm 5$.

In Figure 2*a*, we show the cross-correlation function (CCF) of $F(1826)$ with $F(1338)$, and, as a reference, the autocorrelation function (ACF) of $F(1338)$. Throughout, linear interpolation between the observations is used to construct uniformly sampled light curves, and the errors on the lags are estimated by the method of Gaskell and Peterson (1987). We have also checked that interpolation is justified with the present data (eq. [7] of Gaskell and Peterson). The CCF is virtually undistinguishable from the ACF. It peaks at 0 ± 63 days, with a correlation coefficient $r = 0.991$. The absence of a significant lag and the large value of r imply that $F(1826)$ and $F(1338)$ vary together, suggesting that the same physical mechanism is responsible for the continuous emission at both wavelengths. In Figure 2*b*, $F(1826)$ is plotted as a function of $F(1338)$. As

TABLE 2

LINE AND CONTINUUM INTENSITIES

JD	F(1338)	F(1826)	Lyα1216	CIV1550	MgII2800	FES
	10^{-14} erg.cm^{-2}.s^{-1}.A^{-1}		10^{-14}	erg.cm^{-2}.s^{-1}		Cts
677	15.00±0.54	9.97±0.20	2097	691	274	89
687	...	...	...	...	271	94
723	22.79±1.51	14.92±0.44	2732	869	311	98
726	25.00±1.14	14.48±0.27	S	685	...	97
891	18.52±0.58	12.83±0.31	2798	763	333	94
941	18.16±1.39	11.46±0.54	2830	801	394	100
956	16.63±1.53	11.72±0.35	2957	842	...	98
1414	12.35±2.05	8.06±0.23	2682	757	233	74
1448	15.36±1.28	7.70±0.29	2276	783	275	73
1605	7.66±0.74	5.42±0.30	2047	763	363	67
1659	8.54±0.41	5.61±0.12	S	681	308	60
1694	9.18±1.01	5.67±0.37	1815	667	...	58
1757	9.02±0.42	5.89±0.17	2053	805	272	59
1947	8.43±0.70	5.28±0.37	1920	668	...	57
1957	7.45±0.47	5.28±0.27	1955	721	318	59
1966	7.28±1.07	5.16±0.48	1632	599	309	61
2022	7.65±0.98	5.70±0.58	2083	700	311	52
2026	7.26±1.11	5.03±0.49	1929	727	...	57
2046	8.48±0.54	5.19±0.32	1918	707	...	..
2090	...	...	...	...	289	53
2093	12.61±0.62	7.50±0.33	S	990	...	49
2138	6.86±0.64	4.03±0.20	1604	584	269	44
2169	8.28±0.63	4.94±0.43	1561	592	335	57
2180	8.12±0.74	4.82±0.20	1719	627	255	44
2237	6.84±3.11	3.14±1.45	1888	631	...	79
2247	5.45±1.10	3.02±0.53	1526	651	333	59
2251	4.58±0.86	3.32±0.39	1719	665	...	59
2266	5.92±1.16	2.67±0.63	1509	660	...	55
2282	6.10±0.26	4.12±0.33	1723	684	252	60
2329	...	...	...	...	S	48
2618	2.26±0.14	1.61±0.11	842	410	167	39
2622	2.44±0.30	1.53±0.15	837	427	182	35
2819	1.21±1.45	.49±0.72	713	299	...	45
2943	.85±0.64	.77±0.21	518	182	110	51
2991	.92±0.80	.63±0.13	218	116	...	36
2995	.80±0.34	.68±0.20	303	175	68	..
2999	1.14±0.40	.82±0.17	359	197	123	..
3003	.64±0.37	.72±0.11	389	142	...	..
3186	2.06±0.24	1.52±0.23	574	275	S	37
3272	3.00±0.36	2.10±0.18	793	360	178	49
3337	4.41±0.50	2.96±0.16	939	431	...	..
3370	3.89±0.23	2.49±0.17	1010	422	187	48
3426	2.41±0.28	1.83±0.05	865	408	168	47
3533	4.42±0.39	2.87±0.31	869	447	159	37
3542	4.98±0.53	3.49±0.15	941	400	199	42
3564	6.35±0.36	4.00±0.11	1056	439	192	43
3620	6.05±0.60	4.03±0.23	1257	461	213	40
3654	3.21±0.32	2.36±0.14	942	409	...	46
3729	4.86±0.49	3.21±0.27	1025	470	198	42
3731	5.08±0.36	3.49±0.19	1078	442	194	44
3794	3.71±0.15	3.24±0.27	1016	443	185	52
3821	6.29±0.25	4.24±0.15	1150	485	201	50
3924	6.08±0.43	4.24±0.37	1186	566	172	49
3963	7.73±0.34	5.05±0.18	1273	512	183	51

expected, this shows an excellent correlation, significant at much better than a 99.9999% confidence level. A linear fit to the data yields:

$$F(1826) = (0.63 \pm 0.02)F(1338) + (0.20 \pm 0.12)\,,$$

with a reduced $\chi^2 = 0.73$. Note that throughout we use a minimization technique which takes into account the errors on both variables simultaneously (York 1966). The intercept of the best-fit regression line is small compared to both $F(1826)$ and $F(1338)$ and does not differ significantly from zero. In other words, $F(1826)$ and $F(1338)$ are nearly proportional which means that despite huge flux variations the ultraviolet continuum retained a constant spectral slope. Of course, errors on individual α at any epoch are such that we cannot rule out the existence of small spectral changes. On the other hand, the data do *not* require such variations: the hypothesis that the

TABLE 3

NEAR-IR FLUXES OF FAIRALL 9

JD	J (mJy)	H (mJy)	K (mJy)	L (mJy)
3476..........	16.90	26.42	37.50	72.11 ± 5.12
3608..........	19.95	28.97	39.26	70.14 ± 3.16
3662..........	19.23	30.06	41.88	74.82 ± 4.67
3690..........	20.51	31.77	43.45	74.13 ± 5.27
3767..........	22.08	32.36	45.92	75.51 ± 3.40
3777..........	20.32	33.57	45.50	81.28 ± 6.47
3847..........	19.23	30.90	45.50	63.39 ± 9.19
3850..........	20.14	31.77	43.05	74.82 ± 4.67
3984..........	22.49	34.83	49.43	85.90 ± 2.34
3985..........	22.49	35.16	50.82	71.45 ± 3.22

spectrum varies stands a 93% chance of being wrong in a χ^2 test and a 40% chance in a Kolmogorov test. More important, such variations, if they exist, are not related to the source luminosity.

We have chosen to parametrize the UV slope in two ways: a power-law spectral index α ($F_\nu \propto \nu^\alpha$) and a blackbody temperature T_{bb}. We find $\alpha = -0.52 \pm 0.11$. Galactic and Magellanic stream reddening toward F9 derived from H I 21 cm maps (Burstein and Heiles 1982; Mathewson, Cleary, and Murray 1974) is low ($E[B - V] < 0.04$). The observed soft X-ray absorbing column yields a total extinction $E(B - V) \sim 0.07$ (Morini *et al.* 1986). After correction for reddening (Seaton 1979), the spectral index becomes $\alpha = -0.46 \pm 0.11$, in excellent agreement with the value of Morini *et al.* (1986; $\alpha = -0.40 \pm 0.11$ in 1983). Such a flat ultraviolet continuum seems to be a common feature of many Seyfert 1 galaxies such as NGC 4151 ($\alpha = -0.17 \pm 0.12$; Clavel *et al.* 1987), Akn 120 or NGC 5548 (Wamsteker *et al.* 1984). The reddening corrected blackbody temperature is $26,500 \pm 900$ K. This is interestingly close to the mean value $T_{bb} \sim 26,000$ K, which Edelson and Malkan (1986) find for their sample of Seyfert I galaxies and QSOs by fitting their spectral energy distribution from the millimeter range to the ultraviolet. The SED of F9 is shown in Figure 8 (see Appendix for details). Like most of the Seyfert 1 galaxies studied by Edelson and Malkan, it shows a strong ultraviolet excess or "bump" whose maximum is somewhere in the unexplored EUV region. As pointed out in the introduction, the origin of the bump is not known, but it is probably relevant that T_{bb} is about the same in all active galaxies. It is at least equally important that in F9, T_{bb} sticks to this "magic" value of 26,500 K, despite huge flux variations. This is clearly a new result which sets strong observational constraints on the origin of the ultraviolet continuous emission in AGNs.

Irrespective of its shape and origin, can the UV continuum account for the variations of the optical flux? As can be judged from Figure 1, the amplitude of the variation is one order of magnitude smaller in the FES band than at ultraviolet wavelengths: $f = 2.86 \pm 0.27$. Nevertheless, the shape of the light curves is very similar, suggesting that the emission processes in the two wavebands are closely related. This is better illustrated in Figure 3 where we plot the cross-correlation function of F(FES) with F(1338). The FES and 1338 Å continuum flux are correlated at better than the 99.99% confidence level. Moreover, the CCF is almost undistinguishable from the autocorrelation function of F(1338). Its centroid lies at lag of $+6 \pm 86$ days, not significantly different from zero, and its maximum is $r = 0.95$. This means that the variations in the optical can be fully accounted for by an extension of the UV continuum.

It remains to be explained why f is ~ 10 times smaller in the optical than in the ultraviolet. We have shown above that the continuum varies with a constant spectral slope in the UV. If this remains true through the optical range, it should contribute at most three counts to the FES flux when F9 is at a minimum. The multiperature photometry of Griersmith and Visvanathan (1979), together with the FES calibration of Holm and Crabb (1979), suggest ~ 15 counts for the flux from the underlying stellar population in F9 (see Appendix). The total residual FES flux during low states should therefore be ~ 18 counts, which is only about half of the observed counts at minimum. This could indicate that the galaxy is brighter than expected, i.e. the existence of a photometrically and dynamically detached stellar nucleus as in M31 (Light, Danielson, and Schwarzchild 1974; Kormendy 1987) or M32 (Kormendy 1988). Alternatively, the excess flux could be due to the optical extension of the "steep IR power law" which Edelson and Malkan (1986) and Carleton *et al.* (1987) invoke in their decomposition of the SED of AGNs, and whose intensity is apparently constant (Edelson and Malkan 1987).

b) Dust Emission in the Near-Infrared

The K light curve is again very similar in shape to that of F(1338). However, a close inspection of Figure 1 suggests that the variations at 2.1 μm lag behind those in the ultraviolet. This is confirmed by Figure 4, where we plot the CCFs of $F(J)$, $F(H)$, $F(K)$, and $F(L)$—the flux measured at 1.15, 1.58, 2.10 and 3.35 μm, respectively—with F(1338): indeed, the CCF of $F(K)$ peaks at a lag of 385 ± 100 days with a high correlation coefficient $r = 0.911$. Equally important, the lag seems to be wavelength dependent, increasing from -20 ± 100 ($r = 0.910$) at J, to 250 ± 100 ($r = 0.907$) at H, and 410 ± 110 days ($r = 0.886$) at L. To check the reality of these lags further, we have performed a cross-correlation analysis of the J and K light curves. As expected, K lags behind J by 330 ± 105 days ($r = 0.966$).

Several scenarios could conceivably account for both the UV/IR correlation and the lags. We shall discuss first the most plausible one, namely that thermal reemission by dust of the absorbed UV energy dominates the variations at K and L (and to a lesser extent at H), the J flux being mainly an extension of the UV-optical continuum diluted by stellar light (and possibly by an additional component), hence the absence of a lag. The delays at H, K, and L represent the travel times of the ultraviolet photons and therefore provide a direct estimate of the distance at which the dust shell lies from the continuum source. The range in lags reflects the spatial and temperature distribution of the dust, the grains closer in being hotter and emitting at shorter wavelengths than those further away from the UV source.

Figure 5 lends some credence to this picture; it shows, on a νF_ν versus ν plot, $JHKL$ spectra when F9 is at its maximum (Fig. 5*a*) and minimum (Fig. 5*b*) level of activity. During the bright states there is clearly a peak in the energy distribution at 2.10 μm. As F9 fades, this excess gradually disappears and is replaced by a trough at minimum. In other words, there is an additional and highly variable component which dominates at K and which we attribute to hot dust emission. The 2.1 μm flux deficit at low states is simply a gap between the stellar light which is prominent at J and H and the onset of cool dust emission at L and beyond. The ratios f of the maximum to the minimum fluxes recorded in the IR bands are 1.98 ± 0.08,

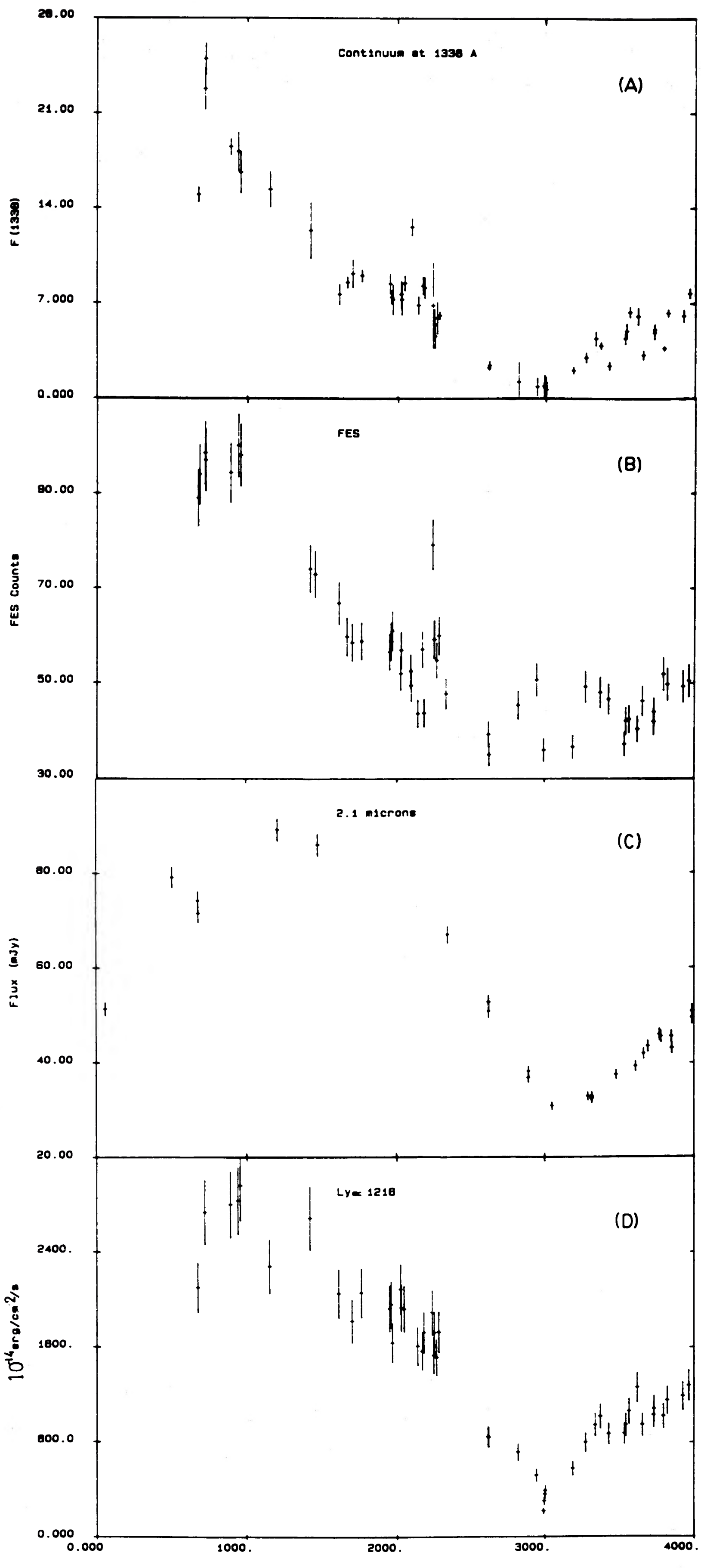

FIG. 1.—Light curves of the UV continuum (*a*) at 1338 Å, *F*(1338), (*b*) in the optical FES band, at 2.10 μm, (*c*) *F*(*K*) and (*d*) of the Lyα 1216 line. Intensities are plotted with their associated error bars. Units are 10^{-14} ergs cm^{-2} s^{-1} Å^{-1} for *F*(1338), counts for the FES flux, mJy for *F*(*K*), and 10^{-14} ergs cm^{-2} s^{-1} for Lyα λ1216. Units on the horizontal axis are Julian days minus 2,443,000. Note the similarity of all four light curves, their amplitude, and their regularity.

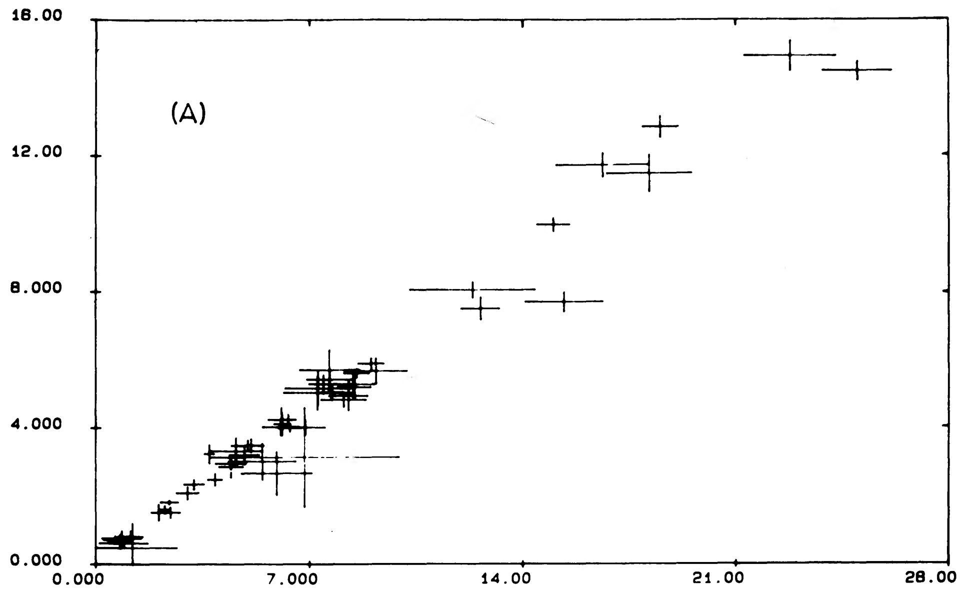

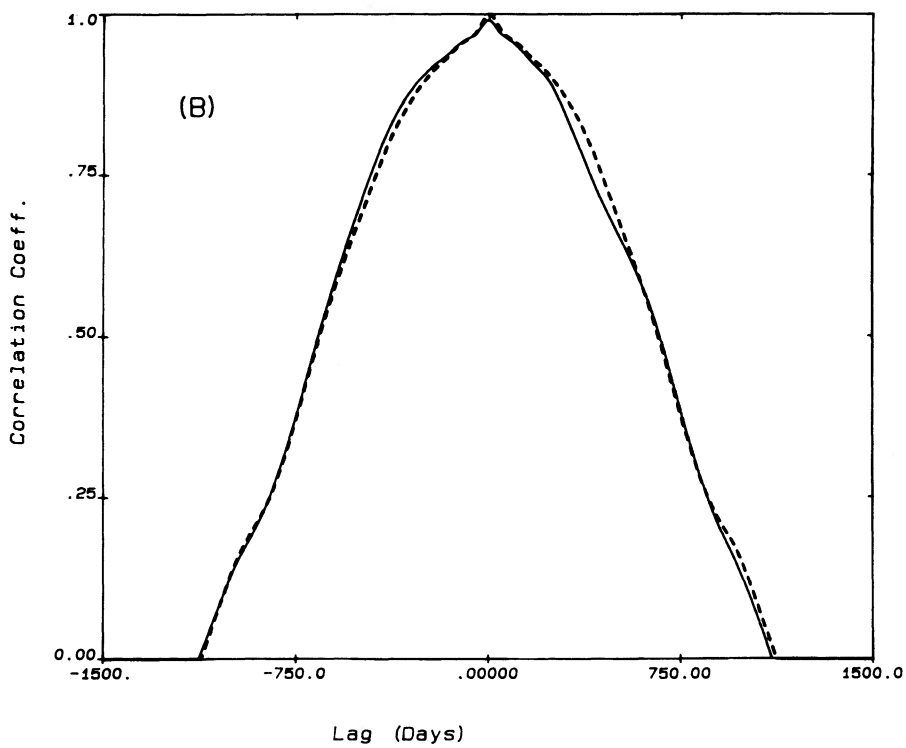

FIG. 2.—(*a*) Intensity of the continuum at 1826 Å, $F(1826)$, vs. that at 1338 Å, $F(1338)$. Units are 10^{-14} ergs cm^{-2} s^{-1}, and are plotted with their error bars. Note the excellent correlation. The best-fit regression line goes through the origin, which implies that the spectral slope of the continuum remains constant, despite the large intensity variations. (*b*) The CCF of $F(1338)$ with $F(1826)$ (*solid line*) and the ACF of $F(1338)$ (*dashed line*) are almost undistinguishable. Hence, there is no delay in the variations at 1826 Å as compared with those at 1338 Å. The large width of the ACF is due to the long time scale (~years) over which quasi-monotonous variations took place.

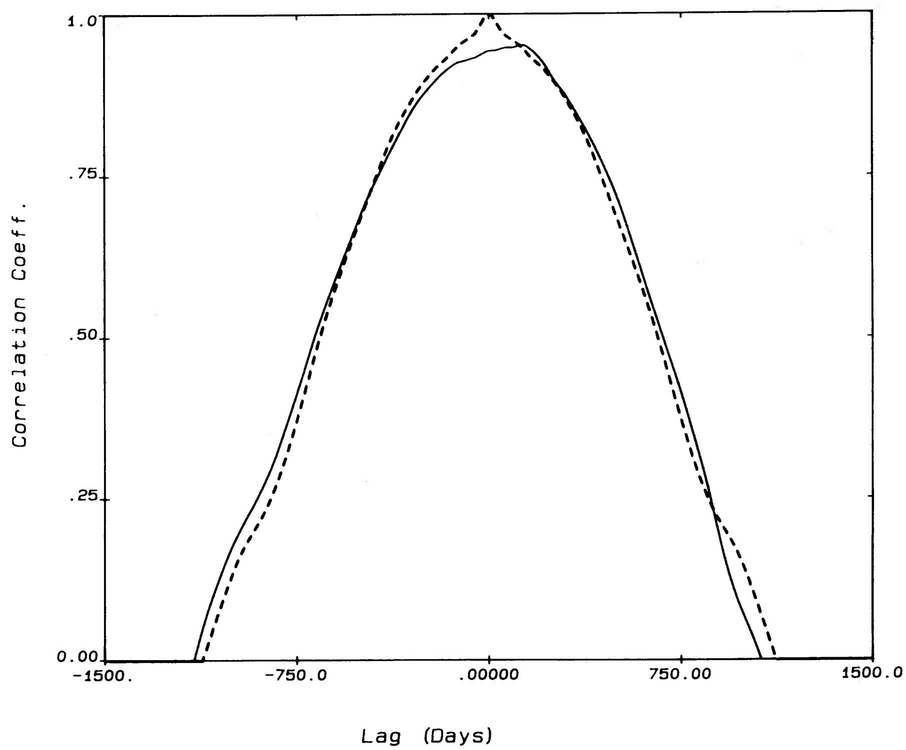

FIG. 3.—CCF of the optical flux, as measured with the FES, and the 1338 Å continuum (*solid line*). Dashed line is the ACF of $F(1338)$. The very high correlation coefficient at the peak of the ACF ($r = 0.95$) and the absence of a lag show that the optical and UV variations are simultaneous. The small shoulder at about +140 days could be due to a minor Balmer line contribution to the FES flux.

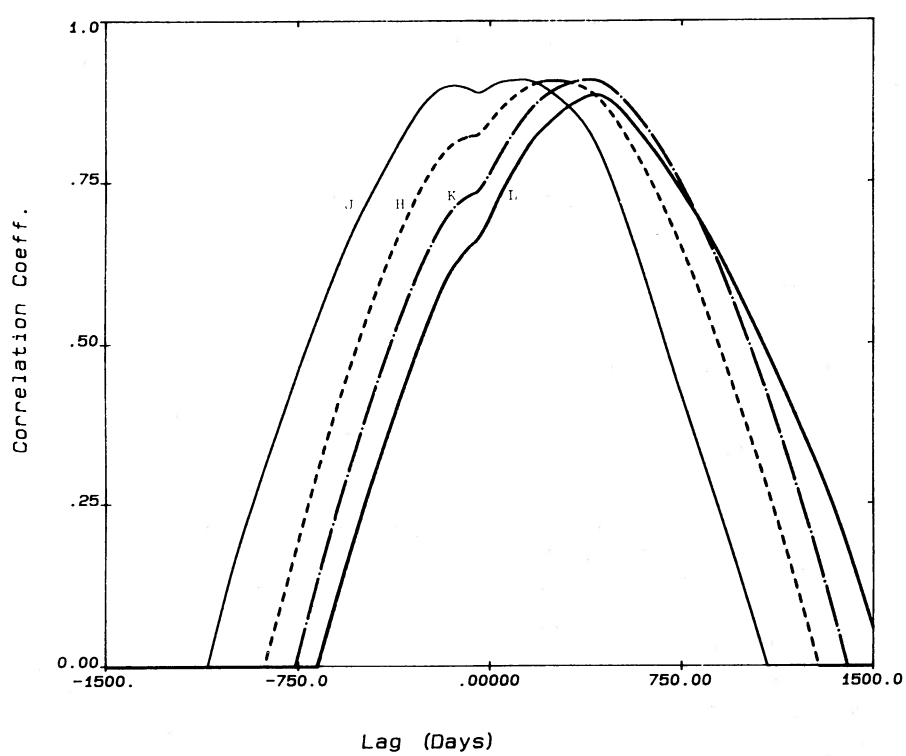

FIG. 4.—The CCF of the fluxes at J (*solid line*), H (*dashed line*), K (*dot-dashed line*), and L (*solid line*) with the UV continuum intensity at 1338Å, showing that the IR flux beyond 1.15 μm lags behind the ultraviolet and that the delay increases with wavelength, up to 410 days at 3.35 μm. We interpret this as evidence for thermal emission from hot dust located at $\sim$400 lt-days from the UV source.

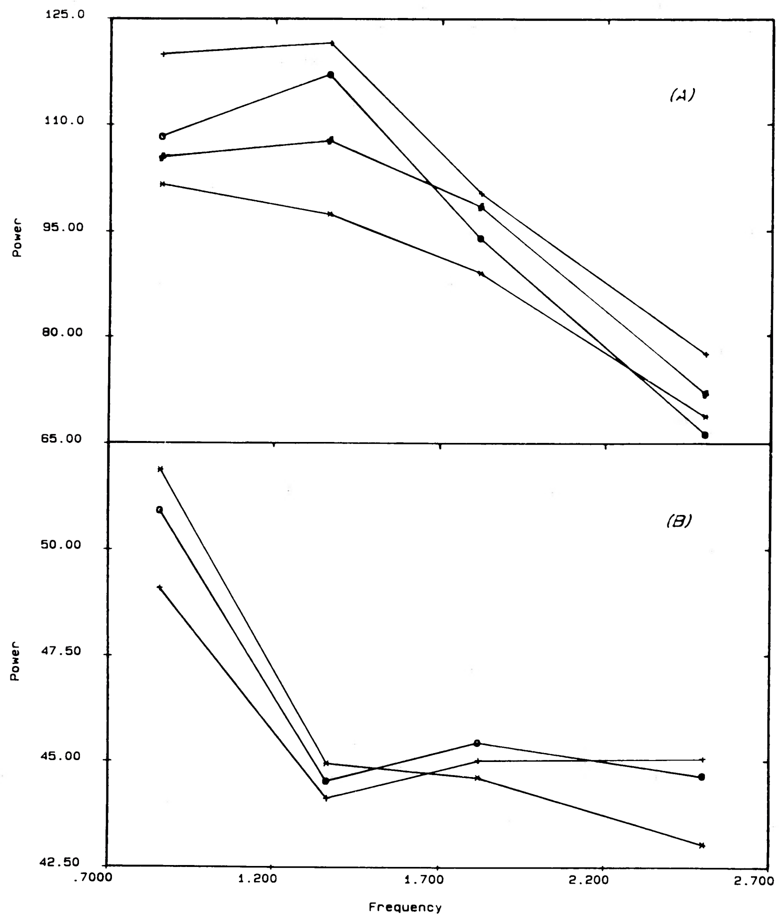

FIG. 5.—*JHKL* spectra at (*a*) the four epochs when F9 is the brightest and (*b*) the three epochs when it is the faintest, plotted on a νF_ν (units of 10^{-12} ergs cm^{-2} s^{-1}) vs. ν (10^{+14} Hz) diagram. This clearly shows that there is an additional emission component which dominates at *K* and which we attribute to hot dust near the UV source. The local minimum at *K* during the low states is simply a gap between the long-wavelength end of the stellar contribution and the onset of cool and nonvariable NLR dust emission at *L*.

2.59 ± 0.10, 2.88 ± 0.11, and 2.44 ± 0.12 at *J*, *H*, *K*, and *L*, respectively, i.e. the variations are the largest at 2.1 μm, presumably because of changes in the hot dust component. At *L*, the flux varies less because of the contribution from cooler dust occupying a much larger volume. The color temperature of the dust is $\sim$1400 K, suggesting that the grains are relatively hot. Knowing the distance *D* of the dust to the continuum source and the UV luminosity, L_{45} (in units of 10^{+45} ergs s^{-1}), it is possible to infer the equilibrium temperature of the grains. In the following, we shall assume that the dust and the gas are symmetrically distributed with respect to the continuum source and that the latter radiates isotropically. Then the lag Δt and the distance *D* are simply related by $D = c\,\Delta t$, where *c* is the velocity of light. Strictly speaking, the lags we measure are lower limits to the propagation time of the photons because the UV-optical continuum is expected to give a direct contribution at zero lag to the observed IR fluxes. This contribution should, however, be small at the longer wavelengths, and in practice the lags at 2.10 and 3.35 μm should yield a reliable estimate of the distance. We have thus adopted:

$$D = 400 \pm 100 \text{ lt-days} ;$$

i.e. the average of the *K* and *L* lags. At such a distance, the grains temperature will be (Barvainis 1987):

$$T_{\rm gr} = 1525\,(L_{45})^{1/5.6} ,$$

where we have assumed a dust optical depth $\tau_{\rm UV} = 0.2$ at 1000 Å. The exact value of $\tau_{\rm UV}$ does not matter as long as it remains small, an assumption which is justified below. A much larger uncertainty is introduced by L_{45} since a correction has to be applied to the measured optical-UV flux in order to take into account the unobservable part of the electromagnetic spectrum of F9 in the $\sim$150–1150 Å range. Following Morini *et al.* (1986), we assume that the flat UV power law extends to 86 eV and then turns over exponentially in order to connect with the soft X-ray excess suggested by the *EXOSAT* observations. The average of L_{45} is 2, yielding

$$T_{\rm gr} = 1730 \pm 230 \text{ K} .$$

The error quoted on $T_{\rm gr}$ assumes a 50% uncertainty in L45 and a 100 lt-day error in *D*, i.e. the adopted uncertainty in the lag. It is interesting that, within the errors, $T_{\rm gr}$ is equal to the (uncertain) sublimation temperature of graphite (1800 K; Rudy and Puetter 1982), the most refractory of all plausible dust constituents. This suggests that the variable IR flux is dominated by emission from the hottest grains, i.e. those which lie just at the dust evaporation radius.

The observed near-IR luminosity can also be used to infer the mass of hot dust present at 400 lt-day. The result is very uncertain, however, since it depends strongly on the assumed grain radius a. Another source of uncertainty is the unknown contribution of the UV-optical continuum at these low frequencies. In the absence of a definite guideline, we have assumed that *all* the observed K flux at high state (after subtraction of the stellar contribution) is due to dust emission. This yields an upper limit to the dust luminosity of $1.6 \times 10^{+30}$ ergs s^{-1} Hz^{-1}. Following Barvainis (1987), we have adopted a radius $a = 0.05$ μm and a mass density of 2.26 g cm^{-3}, appropriate for graphite grains. The assumed dust emissivity and absorption efficiency are also the same as in Barvainis (1987). We obtain 0.02 $M_\odot$ for the mass of hot dust, corresponding to a number of $\sim 3 \times 10^{+46}$ grains. For a galactic gas-to-dust ratio of 200, this yields 4 $M_\odot$ for the mass of gas in the dust region. If the dust is spread in a spherical shell whose thickness is of the order of its radius, then the amount of visual extinction produced is less than 0.02 mag.

The mass of hot dust required is fairly small. However, it is likely to represent only a tiny fraction of the actual amount of dust present in the nucleus of F9. This is because, with the variable K emission, we only sample the "tip of the iceberg," most of the grains being too far away to respond coherently to a change in the level of activity and too cool to emit significantly at 2.1 μm. The very fact that the K and L fluxes keep increasing with increasing UV brightness tells us that the dust shell is geometrically thick and there are always more grains to be heated beyond the evaporation radius. How thick is the shell? Figure 8 shows that the IR bump extends far in the IR. In fact, the F9 bump looks quite similar to that of the *IRAS* discovered QSO 13349+2438, suggesting that the mid- and far-IR as well are dominated by dust emission (Beichman *et al.* 1986). In any case, the 100 μm intensity, together with the I_c ($\lambda_0 \sim 7550$ Å) flux at minimum, leaves little room for an $\alpha \sim -1.5$ power law. If we neglect such a nonthermal contribution and ascribe the whole of the IR emission to dust, the width of the bump (3.5 octaves) and the frequency of its peak ($4 \times 10^{+13}$ Hz), together with Figures 2 and 3 of Barvainis (1987), can be used to infer that the warm dust extends beyond 300 pc, i.e. well into the NLR, with a density profile $n(R) \sim R^{-0.6}$.

We shall now discuss briefly other possible scenarios which could conceivably explain the tight UV/IR correlation and the existence of a wavelength-dependent lag.

Recently, Collin-Souffrin (1987) has proposed a model where the "3 μm bump" characteristic of many AGNs is due to the optically thin emission arising in the outer part of an optically thick geometrically thin accretion disk. Her model is valid only as long as the disk self-gravity remains negligible, which in the optically thin region, sets an upper limit to the accretion rate, $\dot{M} < 0.1\alpha$, where α is the usual viscosity parameter (her eq. [12]bis). In F9, $\dot{M}$ reached 3 M_0 yr^{-1} in 1979 (see § IV). Thus, the above condition can be met only if α exceeds 30. This is inconsistent with the steady disk hypothesis since the turbulence would be highly supersonic, leading to a rapid destruction of the disk.

Another possibility would be that the near-IR flux is free-free radiation from very dense ($N_e > 10^{+11}$ cm^{-3}) BLR clouds which are ionized by the continuum source (Puetter and Hubbard 1985). In this scheme, the lag is simply the time it takes for the UV photons to reach the clouds and be reemitted to the observer. These clouds would therefore be at a distance of 400 lt-days from the nucleus. The main difficulty with this hypothesis is that it requires the dense gas to be *outside* the normal BLR, whose radius is 155 ± 45 lt-day only (see § IV). We have no indication that the BLR density in F9 is significantly larger than the canonical $10^{+9.5}$ cm^{-3}. Therefore, the free-free emission model would imply that the density decreases inward, a situation which is highly improbable.

c) The Broad-Line Region

Figure 1 shows that the light curve of the Lyα λ1216 emission line mimics that of the UV continuum. In Figure 6, we plot the CCFs of the Lyα λ1216, C IV λ1550 and Mg II λ2800 emission lines with $F(1338)$. The maxima are reached at lags of 115 ± 70, 200 ± 80, and 160 ± 90 days, respectively. The corresponding correlation coefficients at the peak are 0.954, 0.858, and 0.883, confirming the tight relation between the UV continuum intensity and the fluxes of the emission lines.

Such a tight relation is expected in photoionization models where the BLR gas is heated and ionized by the central continuum source. The lags are interpreted in terms of light travel times and yield a "radius" for the BLR, i.e. the distance from the UV source at which the bulk of the gas lies.

There are no significant differences in the lags of Lyα λ1216, C IV λ1550, and Mg II λ2800. We have thus adopted:

$$R(\mathrm{BLR}) = 155 \pm 45 \text{ lt-days}$$

for the radius of the BLR in F9. The quoted error is the rms scatter of the individual lags around the mean, and, in the present case, it is equal to the quadratic sum of the individual errors. The BLR is thus considerably more compact than the dust shell. The difference in radius ($\Delta R = 245 \pm 110$ lt-days) is significant at the 98.7% confidence level (i.e. if it was zero, the chance that we would measure such a large value of ΔR is only 1.3%). We conclude that the bulk of the high-velocity gas is free of dust and that the hot grains responsible for the variable near-IR emission lie on the outskirts of the BLR, probably at its interface with the more extended NLR.

Can the line ratios tell us something about the physical conditions in the BLR of F9? The Lyα λ1216/C IV λ1550 and Lyα λ1216/Mg II 2800 intensity ratios are plotted as functions of the UV continuum flux in Figures 7*a* and 7*b*, respectively. The range of variations in Lyα/C IV and Lyα/Mg II define two regions in the line emissivity versus ionization parameter (U) plan which do not overlap: for instance, in the standard model of Mushotzky and Ferland (1984), with a density of 10^{+10} cm^{-3} and column density of $10^{+22.8}$ cm^{-2}, the range spanned by Lyα/C IV requires $-2.50 < \log U < -2.25$, whereas the Lyα/Mg II ratio implies $-1.85 < \log U < -1.40$. For comparison, at the distance we infer for the BLR and for the EUV continuum spectral shape defined earlier, the theoretical value of U varied in the range $\log U \sim -3.0$ to -1.4 during the years 1978–1987. This presumably means that U is not single-valued throughout the BLR at any given time. Rather, the data point toward the existence of a radial distribution in the degree of ionization of the gas.

As Figure 7 shows, there is clearly a trend for both ratios to increase for increasing values of $F(1338)$. A linear fit yields

$$\mathrm{Ly}\alpha/\mathrm{C\,IV} = (0.080 \pm 0.007)F(1338) + (1.96 \pm 0.07)\,,$$

$$\mathrm{Ly}\alpha/\mathrm{Mg\,II} = (0.27 \pm 0.02)F(1338) + (3.89 \pm 0.14)\,,$$

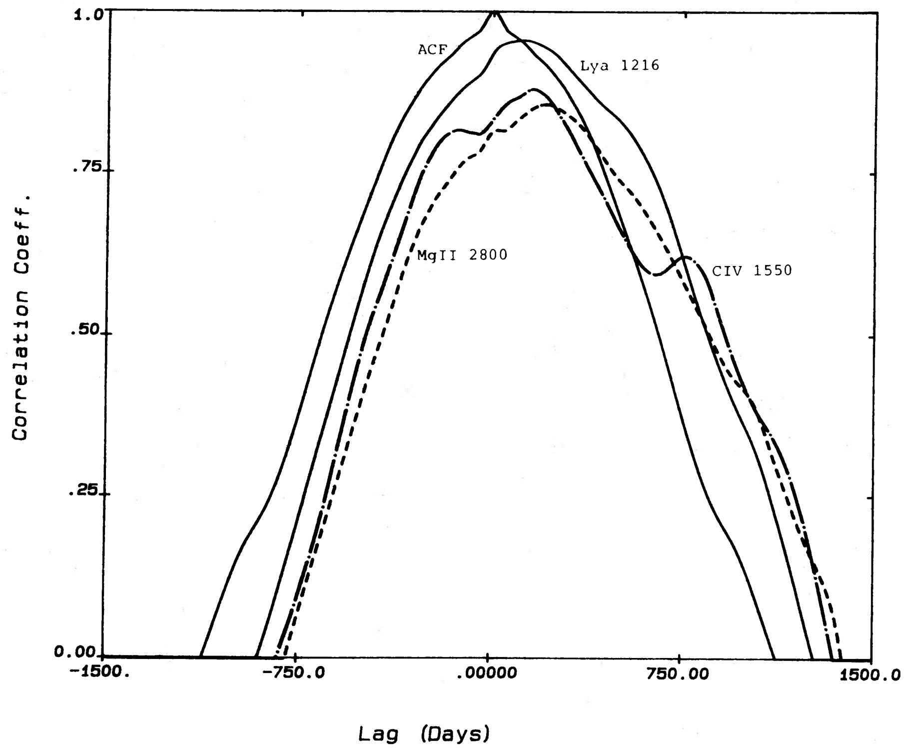

FIG. 6.—The CCF of the Lyα λ1216 (*solid line*), C IV λ1550 (*dot-dashed line*) and Mg II λ2800 (*dotted line*) emission lines with the UV continuum at 1338 Å. The ACF of $F(1338)$ is also shown for reference. All three lines lag behind the continuum by $\sim$155 days. Our interpretation is that the emission-line gas is photoionized and lies at 155 lt-days from the photon source. Note that the correlation coefficient at the peak is significantly higher for the Lyα line (0.95) than for C IV (0.86) or Mg II (0.88), presumably because the later lines are also sensitive to the soft-X ray continuum.

with $r = 0.80$, $\chi^2 = 0.55$ and $r = 0.77$, $\chi^2 = 1.19$, respectively, implying that both correlations are significant at better than a 99.99% confidence level. Such a behavior is apparently at odds with results from photoionized model calculations which predict that both ratios should *decrease* with increasing ultraviolet photon density (see, e.g., Mushotzky and Ferland 1984). However, the contradiction is only apparent. This is because the three lines are sensitive to different parts of the electromagnetic spectrum. The Lyα λ1216 line is mainly excited by photons whose energy lies just above 13.6 eV, whereas the C IV and Mg II lines also respond to higher energy quantas: the C IV λ1550 flux depends on the number of C^{3+} ions and is thus sensitive to the density of photons whose energy is in the range $\sim$48–64 eV. As for Mg II λ2800, the bulk of its flux comes from the warm, partially ionized zone of the cloud, which, according to modern photoionization models of the BLR (Kwan and Krolik 1981; Mushotzky and Ferland 1984) is protected from Lyman continuum photons and receives its energy input mainly from penetrating soft X-rays. Its emissivity depends primarily on the number of photons of $\sim$0.7 keV available to heat that medium. The behavior of the line ratios therefore suggests that *as F9 faded, its spectrum in the EUV soft X-ray range hardened.* There are some hints that this is actually what happened: Figure 4 of Morini *et al.* (1986) shows that from 1978 to 1984 October, the 2–10 keV flux of F9 dropped by a factor 3.5 only, whereas the decline in $F(1338)$ has already reached a factor of 33. In other words, the ratio of X-ray to UV luminosity increased by a factor of $\sim$10 during the fading of F9. Unpublished *EXOSAT* data obtained by us show that the X-ray flux of F9 did not drop further after 1984. Indeed, on 1985 July 26, count rates were 1.06 ± 0.10 counts s^{-1} in the 2–6 keV medium-energy band and 0.073 ± 0.008 and 0.036 ± 0.004 counts s^{-1} in the low-energy LE1 telescope with the thin Lexan and aluminum-parylene filter, respectively. These rates are very similar to those measured by Morini *et al.* during the period 1983 October 11–13, and a factor $\sim$3 higher than in 1984 October. The fact that the emissivity of the C IV λ1550 and Mg II λ2800 emission lines is also sensitive to the density of soft X-ray photons also accounts for the fact that the correlation with $F(1338)$ is not as good for these lines as it is for Lyα λ1216.

Therefore, far from contradicting modern photoionization models, the correlation between line ratios and $F(1338)$ is, on the contrary, a strong argument in favor of such models where the back of each BLR cloud is optically thick and heated by soft X-rays. Moreover, our results imply that the flat UV-optical continuum must roll over at relatively low frequencies in such a way that its contribution to the $\sim$60–700 eV flux does not overwhelm that of the hard X-ray continuum. This is in agreement with the results of Morini *et al.* (1986) who could successfully reproduce the combined simultaneous *IUE* and *EXOSAT* spectra of F9 with a power law of index $\alpha = -0.40$ in the ultraviolet, exponentially cut off at 86 eV, plus a second $a = -0.96$ power-law spectrum above 1 keV. A 26,500 K blackbody spectrum, as found earlier, peaks at 11.7 eV. This is not a difficulty for accretion disk models, however, since realistic calculations predict an emergent spectrum which differs substantially from a pure blackbody. In particular, electron

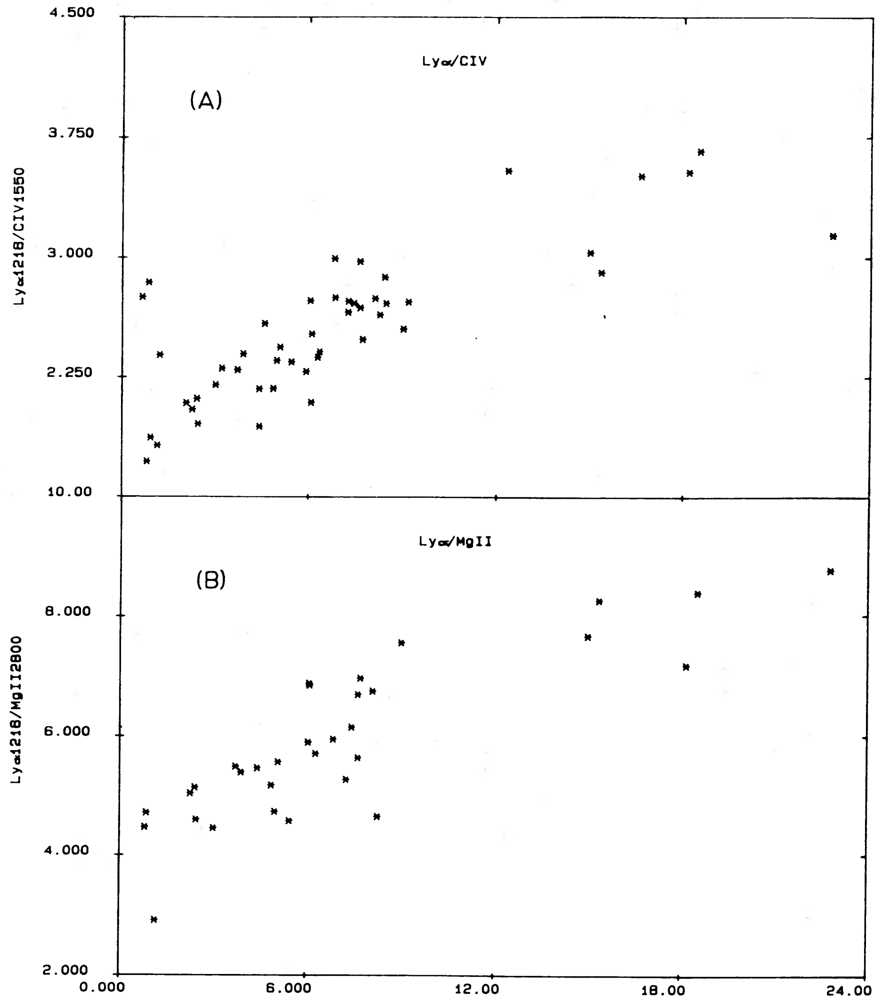

FIG. 7.—(*a*) The Lyα λ1216 over C IV λ1550 and (*b*) Lyα λ1216 over Mg II λ2800 line intensity ratios as a function of *F*(1338), the continuum intensity at 1338 Å. These clearly show good correlations, which are a result of the increase in the X-ray to UV continuum flux ratio during the fading of F9.

scattering and Comptonization are likely to shift the peak of the energy distribution toward higher frequencies, more or less in the range inferred for F9 (Czerny and Elvis 1987).

IV. DISCUSSION

In the hypothesis that the gas clouds are gravitationally bound and follow Keplerian orbits, one can use the previous estimate of the BLR radius to infer the mass inside the nucleus of F9. One has first to assign a characteristic velocity to the BLR material. Whether this velocity should be the half-width at half intensity or the intensity at any other fraction of the flux at the line peak depends entirely on the assumed model, and in particular on the unknown run of emissivity with radius. In the absence of a guideline, we have proceeded as follows: A bright and a faint state spectrum were computed by averaging the data corresponding to the three epochs when *F*(1338) was, respectively, the largest and the smallest. The continua were constructed by linear interpolation of the flux in the 1338 and 1826 Å windows. The line half-widths $D_V/2$ were measured on the difference spectrum " bright minus low state " after subtraction of the continuum. For D_V, we used the velocity interval within which half of the line flux is emitted. This yielded $D_V/2 = 2830$ and 2130 km s^{-1} for Lyα λ1216 and C IV λ1550, respectively. We therefore took the mean of these two values, $D_V/2 = 2500$ km s^{-1}, to be a characteristic velocity of the BLR gas. Combined with $R = 155$ lt-days, this yields:

$$M = 2 \times 10^{+8}\ M_\odot$$

for the mass inside the nucleus of F9. The corresponding Eddington luminosity is $2.5 \times 10^{+46}$ ergs s^{-1}. At its brightest, the luminosity of F9 from the optical to the EUV was $8 \times 10^{+45}$ ergs s^{-1} (see § III*a* for the assumed spectral shape) and $9 \times 10^{+45}$ ergs s^{-1} in the hard X-ray to gamma-ray range. The latter figure assumes that the X-ray spectrum extends up to 1 MeV, with the $\alpha = -0.96$ spectral index measured in the 2–10 keV band (Morini *et al.* 1986). Therefore, the bolometric luminosity of F9 reached at least $1.8 \times 10^{+46}$ ergs s^{-1} or ~70% of the Eddington limit and probably more if one takes into account the unknown mid-to-far-IR nonthermal flux. If the efficiency of conversion of matter into energy is 10%, the accretion rate was as high as 3 $M_\odot$ yr^{-1} in 1978, which immediately rules out Collin-Souffrin's (1987) model of an optically thin disk emission for the origin of the variable IR flux in F9.

Our data also set new constraints on models which aim at explaining the origin of the "big blue bump." Because of its spectral shape which roughly ressembles that of a blackbody and because the existence of accretion disks (AD) in AGNs with about the right temperature is a long-standing prediction (Lynden-Bell 1969), it has become customary to explain the bump in terms of optically thick emission from a geometrically thin accretion disk (Shields 1978; Edelson and Malkan 1986, and references therein). The disk model, however, is plagued by fundamental problems which have been reviewed recently by Antonnuci (1987). Our F9 data add two new difficulties to his list: (1) the ultraviolet spectrum is significantly steeper ($\alpha = -0.46 \pm 0.11$) than the canonical $\nu^{1/3}$ power law predicted by the thin disk theory; (2) large luminosity variations occur at constant effective temperature throughout the UV and probably up to 1 μm, given the absence of a lag in the FES and J light curves. The first difficulty can be overcome by invoking the existence of a hot corona above the disk surface which reprocesses its spectrum. For instance, the model of Czerny and Elvis (1987) predicts $\alpha \sim -0.7$ for the type of black hole mass and accretion rate that we find in F9 if the disk is seen at an inclination of 60°. The second constraint is more difficult to accommodate within the framework of AD models since it implies a readjustment of the temperature of the whole disk, or a large fraction of it. On the one hand, in dwarf novae system such as VW Hydri, where there are good reasons to believe that an AD is the source of the optical-UV radiation, the spectral shape also remains constant during an outburst, except at its onset (Verbunt *et al.* 1987). By analogy, one could claim that the same situation applies in F9. The main difference, however, is that in dwarf novae viscous instabilities can propagate through the disk on the observed variability time scale, whereas this is not possible in F9. The observed two-folding time of the continuum is ~ 130 days. In a geometrically thin optically thick accretion disk, the thermal and the viscous time scales τ(th) and τ(vis) are related in a simple way to the dynamical time scale τ(dyn): $\tau(\text{dyn}) \sim \alpha\tau(\text{th}) \sim \alpha(H/R)^2\tau(\text{vis})$, where α is the viscosity parameter and H/R the relative thickness of the disk at the radius R. Most of the energy is released at ~ 10 gravitational radii where the dynamical time is 1 day in F9. For reasonable values of the viscosity ($10^{-3} < \alpha < 0.1$), τ(th) falls therefore within the range allowed by the observations. The main problem is that a thermal instability is a purely local phenomenon so that it is difficult to understand why the disk *as a whole* should decide to cool down or heat up unless its different parts have had time to exchange information. This exchange cannot proceed faster than the sound velocity. Thus, the minimum time for a change in luminosity throughout the ~ 1200 Å–1 μm spectral region is the viscous time scale, which, given the thin disk hypothesis ($H/R < 0.1$), is an order of magnitude larger than the observed variability time scale. Hence, one is either forced to relax the thin disk assumption or to invoke unrealistically large values of the viscosity parameter.

Recently, Jones and Stein (1987) have investigated a completely different scheme where a UV bump naturally arises due to synchrotron emission from the high-energy secondary electrons which are produced by *pp* collisions in the vicinity of a compact massive object. The constancy of the spectral shape in F9 can probably be accommodated more easily in such a model, since it only requires that the energy spectrum of the relativistic protons remains the same, while only their total number varies. More detailed computations are nevertheless necessary to check if this is indeed possible.

J. C. thanks Luc Binette for an enlightening discussion about the spectral shape of the EUV continuum and the behavior of the line ratios in F9. It is also a pleasure to acknowledge the contribution of D. Kilkenny from SAAO for the $UBVR_cI_c$ photometric measurements. Constructive remarks by an unknown referee are also acknowledged.

APPENDIX

THE SPECTRAL ENERGY DISTRIBUTION IN F9

I. SUBTRACTION OF THE UNDERLYING GALAXY

F9 appears to be an ideal candidate for deconvolution into nuclear and underlying galaxy components since Griersmith and Visvanathan (1979) find a close fit of its radial surface brightness distribution in V to a de Vaucouleurs law:

$$\log (F_\nu) \sim -3.33[(R/R_e)^{1/4} - 1)] ,$$

where $R_e = 9\overset{''}{.}4$ and F_ν is the flux per frequency unit per square arc second. By integrating this formula, the V magnitude of the underlying galaxy can be determined for any aperture with a formal accuracy of about ± 3%. In addition, from its color and morphology, Griersmith and Visvanathan conclude that F9 is an early-type spiral whose luminosity is comparable to that of a first-ranked cluster elliptical.

This exercise has already been performed by Glass (1986), but is repeated here with some improvements. Having derived the V magnitude for the aperture of interest, the $UBVR_cI_cJHKL$ can be found by applying K (redshift) corrections to typical early-type spiral colors. Table 4 shows the actual rest-frame colors and K corrections which have been assumed.

II. SOURCES OF PHOTOMETRY FOR THE SPECTRAL ENERGY DISTRIBUTION

Although much photometry is available for F9, in both the $UBVRI$ and $JHKL$ regions, little of it was obtained at the same time or simultaneously with the *IUE* observations. In order to construct Figure 8, we have selected times when nearly coincidental measurements were available, representative of low, intermediate and high states of the nucleus of F9, as given in the Table 5.

Not much 10 μm or longer wavelength photometry for F9 is available. We include in Figure 8 some 10 μm broad-band and nearby narrow-band points taken by Moorwood (Glass 1986) and some "pointed" *IRAS* data listed in Edelson and Malkan (1987).

TABLE 4

REST FRAME COLORS AND K CORRECTIONS FOR THE GALAXY

Color	Assumed Value[a]	K Correction ($z = 0.0461$)
$U - V$	1.29[b]	0.00[c]
$B - V$	0.90[b]	0.15[d]
$V - R_c$	0.58[e] $\pm$ 0.03	0.06[d,f]
$V - I_c$	1.19[e] $\pm$ 0.06	0.06[f]
$V - K$	3.22[g]	0.23[g,h]
$J - H$	0.78[g] $\pm$ 0.02	0.02[g]
$H - K$	0.22[g] $\pm$ 0.02	0.14[g]
$K - L$	0.22[g] $\pm$ 0.03	−0.06[i]

[a] The errors quoted are estimated standard deviations. They are used to construct the error bars on the nuclear flux after subtraction of the underlying galaxy.

[b] Griersmith 1980.

[c] Correction of U flux is negligible.

[d] Whitford 1971.

[e] Averaged S0 observations of Green and Dixon 1978, who used the Cousins BVR_cI_c system on which the F9 measures were made.

[f] Estimated from Schneider, Gunn, and Hoessel 1983.

[g] Glass 1984.

[h] K-corrected color finally assumed is 3.32 ± 0.10. On day 3313 the measured $V - K$ color was 3.20 ± 0.09 between 9″ and 18″. The predicted and observed values have been averaged.

[i] Longmore and Sharpless 1982.

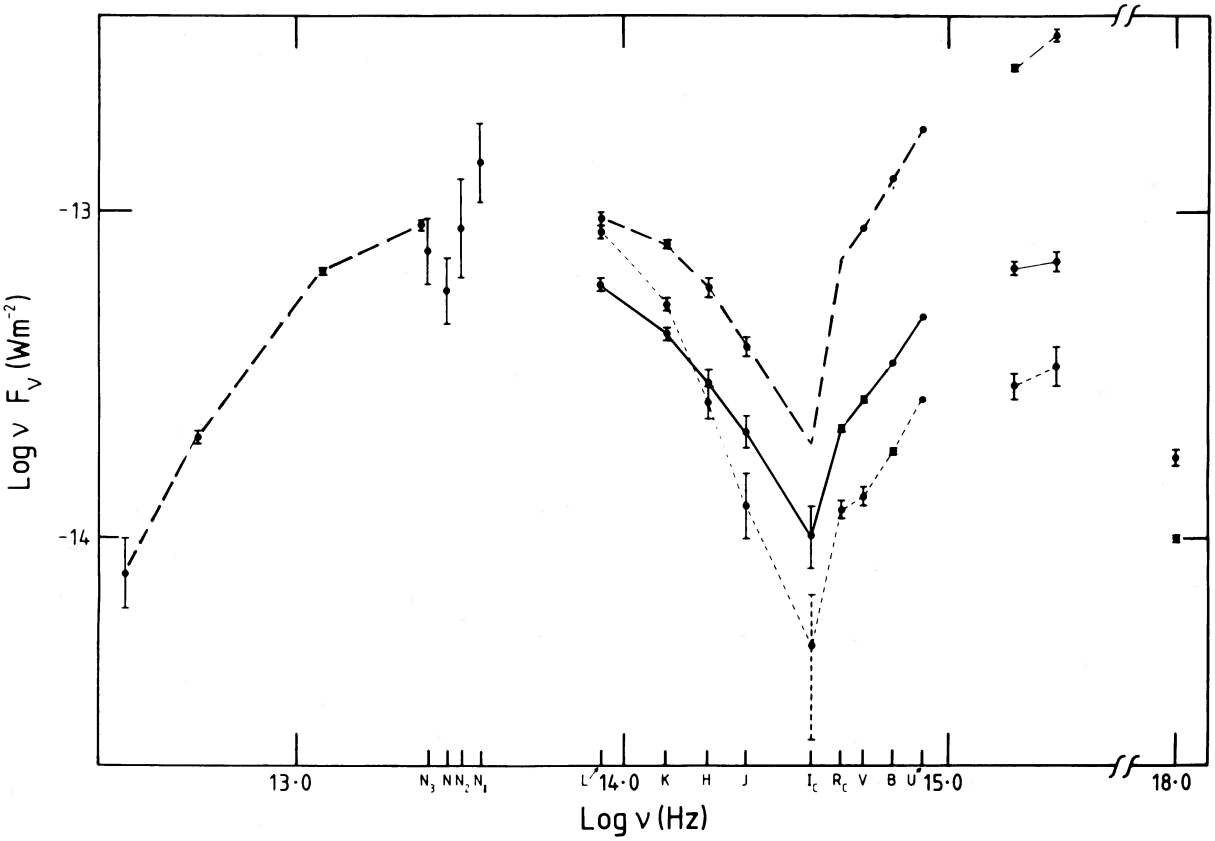

FIG. 8.—Spectral energy distribution of Fairall 9 in νF_ν units after subtraction from the underlying stellar flux (see Appendix for details). The near-IR to far-UV region is shown for three different epochs, representing bright, intermediate, and faint states. Similarly, the X-ray flux is plotted for two epochs. No *IUE* LW points are shown because of the large contamination of Balmer continuum and blended Fe II lines in that range. Good agreement is found between the 12 μm *IRAS* point and the N measurement obtained ~600 days earlier, supporting the conclusion that the variability declines in amplitude toward longer wavelengths. Observed units are used throughout, i.e. without redshift correction.

TABLE 5

DETAILS OF THE PHOTOMETRY REPORTED IN FIGURE 8

High state:
UBV, 15″.4 aperture, day 731 (Griersmith and Visvanathan 1979)
IUE, day 723
JHKL from 12″ aperture; average of day 681 and 683
X-rays, day 671 (Morini *et al.* 1986)
Intermediate state:
UBVRI 16″ aperture day 3770: $V = 13.95$, $B - V = 0.48$, $U - B = -0.81$ $V - R_c = 0.40$, $V - I_c = 0.73$ (D. Kilkenny, private communication)
IUE, day 3794
JHKL, average days 3767 and 3777, 12″ aperture
Low state:
UBVRI, 16″ aperture, day 2620 (J. Menzies; data in Glass 1986)
IUE, day 2621
JHKL, average days 2619, 2620, 2621, 12″ aperture (P. Whitelock; data in Glass 1986)
X-rays, day 2621 (Morini *et al.* 1986)
Other points:
N, N_1, N_2, N_3: 9″ aperture (Moorwood, private communication; data in Glass 1986)
IRAS points, average days 2476 (Edelson and Malkan 1987)

The expected contribution of the underlying galaxy at 60 and 100 μm, obtained from the work of de Jong *et al.* (1984) has been removed.

The relatively large error bars attached to the lower I_c and J points reflect the difficulty of estimating the precise flux from the underlying galaxy which can sometimes amount to almost 90% of the total. Up to 50% of the nuclear R_c band flux can be due to the Hα emission line. The flux calibration for $UBVR_cI_c$ are from Bessel (1979) and for $JHKLN$ from Wilson *et al.* (1972). The N_1, N_2, and N_3 calibrations are interpolated from the latter.

REFERENCES

Antonucci, R. R. I. A. 1987, in *Proc. George Mason University Conf., Supermassive Black Holes*, ed. M. Kafatos (Cambridge: Cambridge University Press).
Arnaud, K. A., *et al.* 1985, *M.N.R.A.S.*, **217**, 105.
Barrylak, M., Watasonic, R., and Imhoff, C. 1985, *ESA IUE Newsletter* No. 20, p. 55.
Barvainis, R. 1987, *Ap. J.*, **320**, 537.
Beichman, C. A., *et al.* 1986, *Ap. J.* (*Letters*), **308**, L1.
Bessel, M. 1979, *Pub. A.S.P.*, **91**, 589.
Boggess, A., *et al.* 1978, *Nature*, **275**, 2.
Bohlin, R. C., and Grillmair, C. J. 1988, *Ap. J. Suppl.*, **66**, 209.
Bohlin, R. C., Holm, A. V., and Lindler, D. J. 1981, *ESA IUE Newsletter*, No. 10, p. 10.
Burstein, D., and Heiles, C. 1982, *A.J.*, **87**, 1165.
Carlton, N. P., *et al.* 1987, *Ap. J.*, **318**, 595.
Clavel, J., *et al.* 1987, *Ap. J.*, **321**, 251.
Clavel, J., Gilmozzi, R., and Prieto, A. 1988, *Astr. Ap.*, **191**, 392.
Collin-Souffrin, S. 1987, *Astr. Ap.*, **179**, 60.
Czerny, B., and Elvis, M. 1987, *Ap. J.*, **321**, 305.
de Jong, T., *et al.* 1984, *Ap. J.* (*Letters*), **278**, L67.
Edelson, R. A., and Malkan, M. A. 1986, *Ap. J.*, **308**, 59.
———. 1987, *Ap. J.*, **323**, 516.
Elvis, M., Wilkes, B. W., and Tananbaum, H. 1985, *Ap. J.*, **292**, 357.
Fairall, A. P. 1977, *M.N.R.A.S.*, **180**, 391.
Gaskell, M., and Peterson, B. M. 1987, *Ap. J. Suppl.*, **65**, 1.
Glass, I. S. 1984, *M.N.R.A.S.*, **211**, 461.
———. 1986, *M.N.R.A.S.*, **219**, 5P.
Green, M. R., and Dixon, K. L. 1978, *Observatory*, **98**, 166.
Griersmith, D. 1980, *A.J.*, **85**, 1295.
Griersmith, D., and Visvanathan, N. 1979, *Astr. Ap.*, **79**, 329.
Holm, A. V., and Crabb, W. G. 1979, *NASA IUE Newsletter*, No. 7, p. 40.
Holm, A. V., *et al.* 1982, *Astr. Ap.*, **112**, 341.
Jones, T. W., and Stein, W. A. 1987, *Ap. J.* (*Letters*), **320**, L1.
Kormendy, J. 1987, in *IAU Symposium 127, Structure and Dynamics of Elliptical Galaxies*, ed. T. de Zeeuw (Dordrecht: Reidel), in press.
———. 1988, *Ap. J.*, **325**, 128.
Kwan, J., and Krolik, J. H. 1981, *Ap. J.*, **250**, 478.
Light, E. S., Danielson, R. E., and Schwarzschild, M. 1974, *Ap. J.*, **194**, 257.
Longmore, A. J., and Sharpless, R. M. 1982, *M.N.R.A.S.*, **201**, 111.
Lynden-Bell, D. 1969, *Nature*, **223**, 690.
Mathewson, D. S., Cleary, M. N., and Murray, J. D. 1974, *Ap. J.*, **190**, 291.
McAlary, C. W., McLaren, R. A., McGonegal, R. J., and Maza, J. 1983, *Ap. J. Suppl.*, **52**, 341.
Morini, M., *et al.* 1986, *Ap. J.*, **307**, 486.
Mushotzky, R., and Ferland, G. J. 1984, *Ap. J.*, **278**, 558.
Netzer, H., and Wills, B. J. 1983, *Ap. J.*, **275**, 445.
Perola, G. C., *et al.* 1986, *Ap. J.*, **306**, 508.
Pounds, K. A., *et al.* 1986, *M.N.R.A.S.*, **224**, 443.
Pravdo, S. H., and Marshall, F. E. 1984, *Ap. J.*, **281**, 570.
Puetter, R. C., and Hubbard, E. N. 1985, *Ap. J.*, **295**, 394.
Rieke, G. H., and Lebofsky, M. J. 1979, **227**, 710.
Rothschild, R. E., *et al.* 1983, *Ap. J.*, **269**, 423.
Rudy, R. J., and Puetter, R. C. 1982, *Ap. J.*, **263**, 43.
Schneider, D. P., Gunn, J. E., and Hoessel, J. G. 1983, *Ap. J.*, **264**, 337.
Seaton, M. J. 1979, *M.N.R.A.S.*, **187**, 73P.
Shields, G. A. 1978, *Nature*, **272**, 706.
Singh, K. P., Garmire, G. P., and Nousek, J. 1985, *Ap. J.*, **297**, 673.
Sonneborn, G., and Garhart, M. P. 1987, *ESA IUE Newsletter*, No. 28, p. 55.
Verbunt, F., *et al.* 1987, *M.N.R.A.S.*, **225**, 113.
Wamsteker, W., *et al.* 1984, in *Proc. 4th European IUE Conf.* (ESA SP-218), p. 97.
Wamsteker, W., Gilmozzi, R., and Clavel, J. 1985, *IAU Circ.*, No. 4081.
Weedman, D. W. 1979, unpublished.
Whitford, A. E. 1971, *Ap. J.*, **169**, 215.
Wilson, W. J., *et al.* 1972, *Ap. J.*, **177**, 533.
York, D. 1966, *Canadian J. Phys.*, **44**, 1079.

JEAN CLAVEL and WILLEM WAMSTEKER: ESA, Apartado: 54065, 28080-Madrid, Spain [Electronic mail: EARN/BITNET: IUEHOT @ ESOC SPAN: ECD1::323VILSPA]

IAN S. GLASS: South African Astronomical Observatory, P.O. Box 9, Observatory, 7935 South Africa